TELKOMNIKA, Vol.11, No.11, November 2013, pp. 6841~6847
e-ISSN: 2087-278X

Detecting and Tracking Hair Impurities in Mushroom Semi-product Images

Wang Xiuping*[1], He Zhongjiao[2]
School of Information & Electronic Engineering, Zhejiang Gongshang University, XueZheng road 18#, Xiasha High Educational Zone, Hangzhou, Zhejiang, P.R. China, 310018
*Corresponding author, e-mail: xpwang@mail.zjgsu.edu.cn[1], he335577@163.com[2]

Abstract

A new area operator was proposed to extract axes feature of hair impurity in mushroom semi-product images. This operator was based on the local intensity comparison, and it had two advantages: 1) its outputs reached local maxima at the hair axes; 2) the accurate direction information of the hair axes could be derived by it. After the axes feature of the hairs was extracted using the proposed operator, an extended Kalman filter was applied to track the hairs. The searching path was established when a cost function was minimized. Starting points of the tracking path were found using dyadic wavelet analysis. The proposed algorithm had good adaptivity for the arbitrary orientation of the hairs. The experiment results showed that hairs could be tracked accurately.

Keywords: *area operator, Kalman filtering, wavelet analysis, feature extraction*

1. Introduction

A computer vision system for recognizing impurities in canned mushroom semi-productions is prevailing for its efficiency. However, literatures about recognizing pieces of hair in complicated backgrounds using computer vision were seldom published. Hair is one kind of common impurities in food products, and can not be detected by common inspection methods such as X-ray. If hairs can be tracked correctly by means of the computer vision, then this technique will be widely utilized in food quality inspection.

In gray-scale images, hairs are characterized by having a ribbon-like or tube-like shape with a pair of closely located parallel edges. Therefore, either the two parallel hair edges or the hair axes are detected in feature extraction [1-5]. Detecting the hair axes is more convenient than detecting the parallel hair edges, because the former needs to track only one line, and the later needs to track two lines. Wavelet analysis can be applied to extract the skeleton of ribbon structure [4-5]. Wavelet methods are computationally efficient, but the accurate information of axes direction can not be obtained directly from them. To address this, a modified SUSAN operator is proposed. The modified SUSAN has positive outputs achieving local maxima on the hair axes, and it can obtain reliable direction information at the same time. Avoiding differentiation and direct working on the intensity value, this operator is resistant to image noise and illumination variation. After the start point is determined by the wavelet methods, a hair tracking algorithm begins to run by using an interactive searching and predicting method. In the searching stage, integrating the direction, the distance, the modified SUSAN output value, and the pixel intensity, the cost function is minimized. In the predicting stage, an extended Kalman filter is utilized.

Section 2 introduces the two hair axes extracting methods: the first one is based on dyadic wavelet analysis and the second one is based on the modified SUSAN operator. The computational efficiency and the informativity of the two feature extracting methods are compared. Section 3 presents the hair tracking algorithm using an extended Kalman filter. Section 4 analyzes the experiment results, and section 5 is the discussion.

Received May 7, 2013; Revised July 21, 2013; Accepted August 5, 2013

2. Local Feature Extraction

2.1. Wavelet Axes

The mushroom semi-product images have complicated edge patterns that consist of mushroom edges, highlight edges, shadow edges and sometimes hair impurity edges. Multi-scale wavelet analysis [6] can be applied to distinguish different kinds of edges. The parallel edges of the hair are detected simultaneously from the pattern of the local maxima in the horizontal and vertical detail wavelet coefficients of 2 scales [4]. Two nearby edges of similar edge strength and opposite gradient directions (a positive followed by a negative one) are considered as candidate hair edge points. The midpoints of the two parallel edges are the candidate hair axes. This method is accomplished with 2-D dyadic wavelet analysis using the bi-orthogonal CDF2-10 wavelet filters. The green points in Figure 1(b) are the results of wavelet axes found from the wavelet maxima whose abstract value are large then $2\sigma_i$. $\sigma_i,\ i = 1, 2, 3, 4$ is the standard deviation of the wavelet coefficients of the correspondent direction (horizontal or vertical) and level (1 or 2).

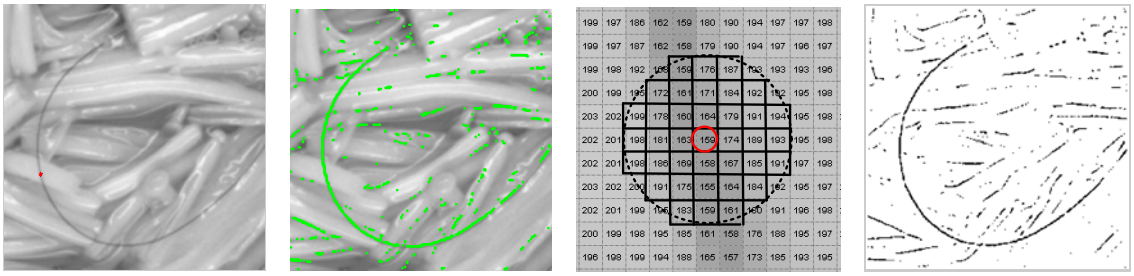

(a) A Grey-scale image. (b) The wavelet axes. (c) 7×7circular mask surrounding the marked pixel in (a). (d) The modified SUSAN local maxima with R>17 and D<1

Figure 1. The Effect of the Modified SUSAN Operator

2.2. Modified SUSAN Operator

Wavelet axes containing only position information are derived from parallel edges. The important information about the direction of the axes is missing. To overcome this difficulty, methods using local information to find the hair axes directly should be proposed [7]. SUSAN operator [8] is excellent for the robust performance in local feature extraction. Useful local features can be detected from the size, centroid and the second order moment of the USAN (Univalue Segment Assimilating Nucleus). Because SUSAN operator is an edge detector other than an axes detector, changes have to be made on this operator to suit for hair axes detection task. Without changing the main process of SUSAN operator, 4 modifications are made on its inner functions. Figure 1 illustrates the effect of the modified SUSAN operator. Using a 7×7 circular mask, which is shown in Figure 1(c), the modified SUSAN operator begins with the brightness comparison between the central pixel (nucleus) and the surrounding pixels.

The first modification is on the comparison function. It is changed to:

$$c(\vec{r},\vec{r}_0) = \frac{\operatorname{sign}\left(\Delta I\right)}{1+\exp\left(-0.5\left(\left|\Delta I\right|-t\right)\right)} \tag{1}$$

Where $\vec{r}_0$ is the position of the nucleus in the two dimensional image, $\vec{r}$ is the position of any other point within the mask, $\Delta I = I(\vec{r}) - I(\vec{r}_0)$, I is the brightness of any pixel and $c(\vec{r},\vec{r}_0)$ is the brightness comparison result between $\vec{r}$ and $\vec{r}_0$, t is the brightness difference threshold. In our experiments, t is set to:

$$t = 0.5 \cdot \sigma_I \tag{2}$$

Where σ_I is the standard deviation of the intensity of the pixels in the 7×7 circular mask.

In Figure 2, the comparison function of Equation (1) is stair shaped with an output range (–1, 1). If the nucleus is much brighter than the neighboring pixel, the output of comparison function is close to –1. If the nucleus is much darker than the neighboring pixel, the output of comparison function is close to 1.

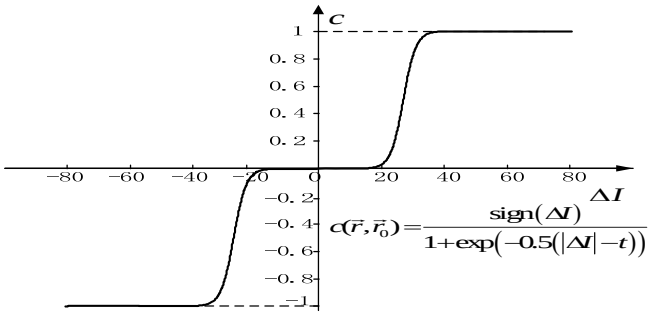

Figure 2. Comparison Function of the Modified SUSAN Operator

The second modification is on the calculation of the total n. This n is the total number of pixels whose brightness differences from the nucleus are larger than the threshold t:

$$n(\vec{r}_0)=\sum_{\vec{r}}|c(\vec{r},\vec{r}_0)| \tag{3}$$

The third modification is on the output function:

$$R(\vec{r}_0)=\begin{cases}\sum_{\vec{r}} c(\vec{r},\vec{r}_0), & \text{when } n(\vec{r}_0)>n_l\\ 0, & \text{otherwise}\end{cases} \tag{4}$$

Where $n_l=n_{\max}/4$, $n_{\max}$ is the maximum value of n. For a 7×7 mask, $n_{\max}=37$. The output $R(\vec{r}_0)$ reflects the difference of pixel intensity between the nucleus and the surrounding pixels.

The fourth modification is on the direction calculation method. We calculate the direction of the axis at each nucleus pixel using eigen decomposition of the correlation matrix $\begin{bmatrix}A & C\\ C & B\end{bmatrix}$:

$$A=\sum_{\vec{r}}\left((x-x_0)^2\cdot|c(\vec{r}-\vec{r}_0)|\right) \tag{5}$$

$$B=\sum_{\vec{r}}\left((y-y_0)^2\cdot|c(\vec{r}-\vec{r}_0)|\right) \tag{6}$$

$$C=\sum_{\vec{r}}\left((x-x_0)\cdot(y-y_0)\cdot|c(\vec{r}-\vec{r}_0)|\right) \tag{7}$$

Let $[P_1,\ P_2]^T$ be the eigen vector of matrix $\begin{bmatrix}A & C\\ C & B\end{bmatrix}$ and P_1 corresponds to the bigger eigen value. The axis direction at $\vec{r}_0$ is:

$$\theta(\vec{r}_0) = \tan^{-1}\left(\frac{P_2}{P_1}\right) = \tan^{-1}\left(\frac{A - B - \sqrt{(A-B)^2 + 4C^2}}{2C}\right) \quad (8)$$

We can also derive centroid information from the modified SUSAN operator: the distance of the "gravity center" from the nucleus is:

$$D(\vec{r}_0) = \sqrt{(\overline{x} - x_0)^2 + (\overline{y} - y_0)^2} \quad (9)$$

Where $\overline{x}$ and $\overline{y}$ are the coordinate of the "gravity center":

$$\overline{x} = \frac{\sum_{\vec{r} \in S} x(\vec{r})\, c(\vec{r}, \vec{r}_0)}{N}, \quad \overline{y} = \frac{\sum_{\vec{r} \in S} y(\vec{r})\, c(\vec{r}, \vec{r}_0)}{N}$$

Where N is the number of elements in the set S. The set S is a set of points with positive $c(\vec{r}, \vec{r}_0)$ in the 7×7 circular area surrounding $\vec{r}_0$:

$$S = \{\vec{r} \mid c(\vec{r}, \vec{r}_0) > 0\}$$

The surrounding area of the pixel marked red in Figure 1(a) is zoomed and illustrated in Figure 1(c), and we can see that its brightness value is 159. The modified SUSAN output of this marked pixel is 28.80, which reaches the local maximum on the direction perpendicular to the hair axis. The direction at this hair axis point is 1.296 in radian and the centriod distance deviation is 1.0568. If we calculate the modified SUSAN output of all the pixels, the pixels whose modified SUSAN output are the local maxima with $R > 17$ and $D < 1$ are plot in Figure 1(d).

The proposed modified SUSAN operator does not work directly on the pixel intensity so that global thresholds are possible to be used. The modified SUSAN operator has several advantages: 1) its output R reaches maximum at hair axis; 2) it is able to provide accurate hair axis direction information θ; 3) the centriod deviation D helps to distinguish asymmetric mushroom shadows from symmetric hair axes.

3. Tracking with Extended Kalman Filter

Kalman filter [9-12] provides a recursive algorithm for the linear optimal filtering problem. The system dynamic is modeled in the state-space formulation, and the measured output is modeled as a linear function of states with additive noise. If the system model is nonlinear, extended Kalman filter (EKF) performs linearization in every step of the recursion.

3.1. System and Observation Models for Hair Tracking

Four state variables are considered in the EKF model, i.e., the position of the hair axes (x, y), the moving ahead distance d, and the current axes direction θ in radian. The state vector is $X_k = [x_k,\ y_k,\ d_k,\ \theta_k]$. The system and observation model are:

$$X_{k|k-1} = A_{k-1} X_{k-1} + W_{k-1} \quad (10)$$

$$Y_{k-1} = C X_{k-1} + V_{k-1} \quad (11)$$

Where W is state dynamic noise and V is observation noise. The state transition matrix A is updated on every step of recursion:

$$A_{k-1}=\begin{bmatrix}1 & 0 & \cos\theta_{k-1} & -d_{k-1}\sin\theta_{k-1}\\ 0 & 1 & \sin\theta_{k-1} & d_{k-1}\cos\theta_{k-1}\\ 0 & 0 & 1 & 0\\ 0 & 0 & 0 & 1\end{bmatrix} \tag{12}$$

The observation matrix C is:

$$C=\begin{bmatrix}1 & 0 & 0 & 0\\ 0 & 1 & 0 & 0\\ 0 & 0 & 0 & 1\end{bmatrix} \tag{13}$$

At every step of recurrence, after obtaining the two observations $\tilde{x}_{k-1}$ and $\tilde{y}_{k-1}$, the other observation variable $\tilde{\theta}_{k-1}$ can be calculated using Equation (8). We set some constants in the system by comparing experiment results. The variance of system dynamic noise is chosen to be $Q_s = \mathrm{Cov}(W) = \mathrm{diag}([0,\ 0,\ 0.4,\ 0.2])$. The variance of observation noise is set to: $Q_o = \mathrm{Cov}(V) = \mathrm{diag}([1,\ 1,\ 0.5])$. When the initial values are set and the observation vector is obtained, the extended Kalman filter can be computed recursively, as described in [9].

3.2. Tracking Process

Given the starting point (x_0, y_0), the initial value of the state vector is $X_0 = [x_0,\ y_0,\ 1, \theta_0]$, where θ_0 is calculated by Equation (8). The initial observation vector value is $Y_0 = [x_0,\ y_0, \theta_0]$. The state vector's filtering error covariance matrix P is initialized as the variance of the observation $P_0 = \mathrm{diag}([1,\ 1,\ 2,\ 0.5])$. Then we can estimate the next state vector X_1 and update the state transition matrix to obtain A_1 by EKF algorithm. A small-scaled searching procedure is performed to find the observation vector Y_1. The observation vector is obtained by searching in the neighborhood of the predicted position at very step of the EKF recursive algorithm. The predicted position is:

$$\hat{x}_k = x_{k-1} + d_{k-1}\cdot\cos\theta_{k-1} \tag{14}$$

$$\hat{y}_k = y_{k-1} + d_{k-1}\cdot\sin\theta_{k-1} \tag{15}$$

As illustrated in Figure 3, the problem is to find the best observation point $N(\tilde{x}_{k-1}, \tilde{y}_{k-1})$, minimizing a cost function:

$$\underset{\tilde{x}_k,\tilde{y}_k}{Min}\quad J = c_1\cdot d_1 + c_2\cdot\Delta\theta + c_3\cdot I_N - c_4\cdot R_N \tag{16}$$

$$s.t.\ \ d_1 < 4,\ \ d_2 < 4,\ \left|\Delta\theta\right| < \pi/4 \tag{17}$$

$$\left|\tilde{x}_k - \tilde{x}_{k-1}\right| + \left|\tilde{y}_k - \tilde{y}_{k-1}\right| \neq 0 \tag{18}$$

Where I_N is the pixel intensity of the point N, R_N is the modified SUSAN output of N, and c_1 ~ c_4 are preset weights.

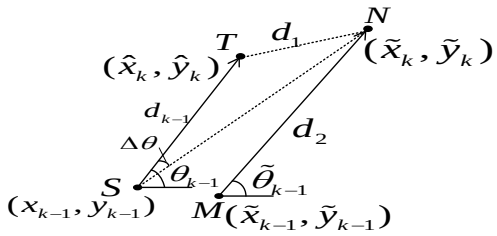

Figure 3. Illustration of the Spatial Relations between the State Variables and the Observation Variables in Hair Tracking with EKF

The tracking method described above shows that the modified SUSAN operator not only provides the direction information $\tilde{\theta}_k$ for observation variables, but also plays an important role in the searching procedure.

4. Experiment Results

The hair pieces' diameter is about $75\mu m$. In experiments, we use a DH-SV2000FC camera with a Kowa LM8JCM lens. DH-SV2000FC is a color camera with a 1/1.8″ sensor and its resolution is 1628×1236. The field of view is $100mm$ and the working distance is $200mm$. The minimum distinguishable feature size of the object under inspection is $83\mu m$. Limited by the system cost, the selected camera's resolution is a bit less than that required by the experiment.

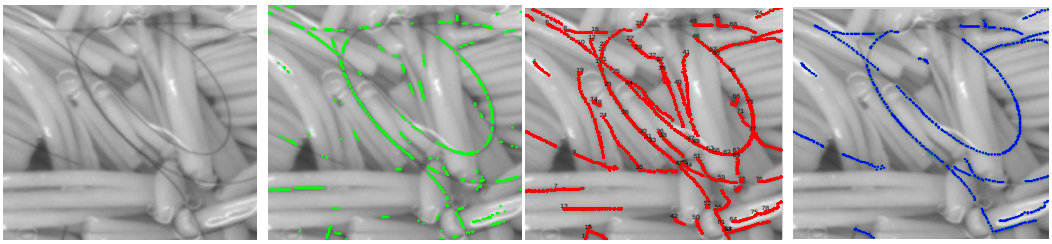

(a) Original image (b) Candidate starting points of wavelet axes (c) All of the tracking paths (d) The result after simple selection

Figure 4. Hair Tracking Procedure and Result

After the image acquisition, the candidate points of hair axes are obtained using a 2D dyadic wavelet transform. Then points with modified SUSAN output $R > 12$ are selected as the starting points for tracking. During the tracking procedure, if the tracked points are contained in the starting points set, they are removed so that no point is tracked more than once. An original image with multiple hair pieces is shown in Figure 4(a). Green points in Figure 4(b) are the candidate hair axes and all of the tracking paths are illustrated in Figure 4(c). The result shown in Figure 4(d) is obtained simply by choosing the paths with the average modified SUSAN output $R > 15$ and the average centroid deviation $D < 1.25$. All of the hair pieces are tracked correctly in Figure 4(c). Because the selection criterion is too simple, the result is not fully satisfactory. As illustrated in Figure 4(d), line 4, 64, 74, 78 are all shadows caused by high lights and are confused with hair axes.

5. Discussion

The wavelet based method of hair axes extraction is computationally efficient, but it can not provide the direction information for the detected axes. The modified SUSAN needs more

computational efforts, but it can provide more useful information for local feature extraction. The axes direction information derived by the modified SUSAN is very accurate. An EKF is used to combine these two methods to solve the problem of hair impurities detection and tracking in clutter background made up of juicy mushroom semi-products. According to the characteristics of the hair axes directions and the statistical regularities of the prediction error, the hair axes are predicted in a leapfrogging way, and point-by-point connection is unnecessary, which are the advantages of the EKF method. If the hair is slightly occluded, hair tracking results are not affected. Therefore, the hairs tracked by EKF method are continuous and integral.

To get more satisfactory results, much work will be done in future. Generally, the hair axes are smooth curves with slow changing curvatures, and the curvature information is not used in the EKF method. After tracking paths are determined by the EKF method, curvature information can be easily calculated from the axes direction information. Then further selections based on curvature information can be made. To get rid of the confusable mushroom edges, a better threshold choosing method, i.e., local thresholding method, for the modified SUSAN should be put forward. Moreover, other feature such as color can also be used in the EKF method.

Acknowledgements

This work was supported by the ZheJiang Province's Office of Science and Technology's Public Welfare Technology Research of Industrial Project of China under Grant Nos. 2010C31009), the ZheJiang Province's Natural Science Foundation of China under Grant Nos. LY12F05004).

References

[1] Zhang Q, Couloigner I. Accurate Centerline Detection and Line Width Estimation of Thick Lines Using the Radon Transform. *IEEE Transactions on Image Processing*. 2007; 16(2): 310-316.
[2] Mendonça AM, Campilho A. Segmentation of Retinal Blood Vessels by Combining the Detection of Centerlines and Morphological Reconstruction. *IEEE Transactions on Medical Imaging.* 2006; 25(9): 1200–1213.
[3] Berlemont S, Olivo-Marin JC. Combining local filtering and multiscale analysis for edge, ridge, and curvilinear objects detection. *IEEE Transactions on Image Processing.* 2010; 19(1): 74-84.
[4] Wang X, Li T. *Image Feature Extraction for Hair Pieces Detection in Mushroom Semiproducts*. Proceedings of the First IEEE International Conference on Information Science and Engineering (ICISE '09). Nanjing. 2009: 1282-1286.
[5] Tang YY, You X. Skeletonization of Ribbon-Like Shapes Based on a New Wavelet Function. *IEEE Transactions on Pattern Analysis and Machine intelligence*. 2003; 25(9): 1118-1133.
[6] Mallat S, Zhong S. Characterization of signals from multiscale edges. *IEEE Transactions on Pattern Analysis and Machine Intelligence*. 1992; 14 (7): 710-732.
[7] Carlotto MJ. Enhancement of Low-Contrast Curvilinear Features in Imagery. *IEEE Transactions on Image Processing*. 2007; 16(1): 221-228.
[8] Smith SM, Brady JM, SUSAN. A New Approach to Low Level Image Processing. *International Journal of Computer Vision*. 1997; 23(1): 45-78.
[9] Haykin S. Kalman filtering and neural networks. New York: John Wiley & Sons, 2001. 16-20.
[10] Chutatape O, Zheng L, Krishnan SM. *Retinal blood vessel detection and tracking by matched Gaussian and Kalman filters*. IEEE 20th International Conference on Engineering in Medicine and Biology Society. Hong Kong. 1998: 3144-3149.
[11] Dai H, Dai S, Cong Y, Wu G. Performance comparison of EKF/UKF/CKF for the tracking of ballistic target. *Telkomnika*. 2012; 10(7):1692-1699.
[12] Yu J, Jin X, Wang G. Vision-aided navigation for autonomous aircraft based on unscented Kalman filter. *Telkomnika*. 2013; 11(2):1093-1100.